This is an open access article published under a Creative Commons Attribution (CC-BY) License, which permits unrestricted use, distribution and reproduction in any medium, provided the author and source are cited.

ACS OMEGA

Article

Cite This: ACS Omega 2018, 3, 8655−8662

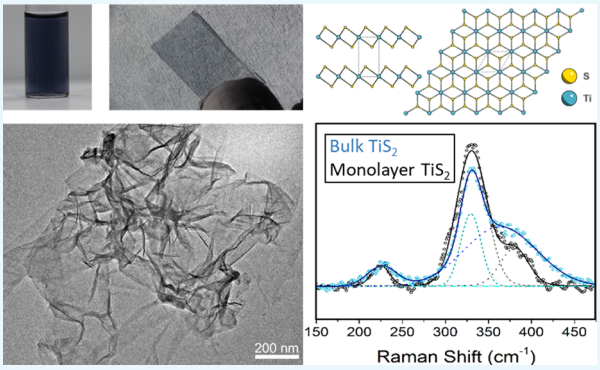
Thickness-Dependent Characterization of Chemically Exfoliated TiS_2 Nanosheets

Peter C. Sherrell, Kanudha Sharda, Chiara Grotta, Jacopo Ranalli, Maria S. Sokolikova, Federico M. Pesci, Pawel Palczynski, Victoria L. Bemmer, and Cecilia Mattevi*

Department of Materials, Imperial College London, London SW7 2AZ, U.K.

Supporting Information

ABSTRACT: Monolayer TiS_2 is the lightest member of the transition metal dichalcogenide family with promising applications in energy storage and conversion systems. The use of TiS_2 has been limited by the lack of rapid characterization of layer numbers via Raman spectroscopy and its easy oxidation in wet environment. Here, we demonstrate the layer-number-dependent Raman modes for TiS_2. 1T TiS_2 presents two characteristics of the Raman active modes, A_{1g} (out-of-plane) and E_g (in-plane). We identified a characteristic peak frequency shift of the E_g mode with the layer number and an unexplored Raman mode at 372 cm^{-1} whose intensity changes relative to the A_{1g} mode with the thickness of the TiS_2 sheets. These two characteristic features of Raman spectra allow the determination of layer numbers between 1 and 5 in exfoliated TiS_2. Further, we develop a method to produce oxidation-resistant inks of micron-sized mono- and few-layered TiS_2 nanosheets at concentrations up to 1 mg/mL. These TiS_2 inks can be deposited to form thin films with controllable thickness and nanosheet density over square centimeter areas. This opens up pathways for a wider utilization of exfoliated TiS_2 toward a range of applications.



INTRODUCTION

Transition metal dichalcogenides (TMDs) are layered materials, which have recently attracted great interest because of their tunable electronic structure with the layer number.[1−3] Titanium disulfide (TiS_2) belongs to this family and in its layered bulk form has attracted interest since the early 1980s as an electrode material for lithium-ion batteries.[4−7] TiS_2 crystallizes in an octahedral (1T) phase, which is energetically more stable compared to its hexagonal (2H) phase.[8] A single triatomic sheet of TiS_2 is formed by a Ti atom layer sandwiched between two layers of S atoms covalently bonded to the Ti atoms. In its bulk form, it exhibits a semimetallic behavior, and theoretical calculations for monolayer TiS_2 suggest a similar semimetal behavior with a small overlap of valence band maximum and conduction band minimum.[9] This behavior is strengthened under compressive strain when the band overlap increases, whereas a small indirect band gap starts to emerge under tensile strain.[9] A further increase of the tensile strain leads to a transition from indirect to direct band gap,[9] with the direct band gap ranging between 0.383 and 0.389 eV.[9] Although experimental measurements have repeatedly demonstrated the semimetallic behavior of bulk TiS_2, the monolayer materials have exhibited a semiconducting behavior under standard nonstrain conditions. The discrepancy between the experimental evidence and the theoretical calculations for monolayer TiS_2 has been attributed to the existence of nonstoichiometric TiS_2 (titanium-rich as being $Ti_{1.023}S_2$).[10−12] Atomic defects may also play a role in shifting the behavior to semiconducting.

Along with two-dimensional (2D) TiS_2 nanosheets,[13−15] other nanostructured polymorphisms of TiS_2, such as nanotubes and nanospheres,[16] have attracted renewed interest. The interest is primarily driven by their prospective application in lithium and sulfur batteries[17,18] as the theoretical energy density of the Li−TiS_2 couple is 480 W h/kg[19] and the theoretical capacity is 239 mA h/g.[20] Furthermore, an all-solid-state Li−TiS_2 battery exhibited a power density of 1000 W/kg over 50 cycles with a maximum power density of 1500 W/kg.[20]

Despite an increasing interest in TiS_2, little is known about its properties in the mono- or few-layered form. Raman spectroscopy is a powerful tool in the characterization of TMDs as the vibrational modes often change position, or relative intensity, as TMDs progress from bulk to monolayered.[21−23] However, the Raman modes change with the layer number of TiS_2 and the electronic band structure remains relatively unexplored.

Liquid exfoliation of bulk layered materials is being extensively used for large-scale production of inks of nanosheets with high concentration (up to 40 g/L) in organic solvents or water with surfactants.[24−26] The results of these

Received: April 20, 2018
Accepted: June 19, 2018
Published: August 3, 2018

Downloaded by IMPERIAL COLLEGE LONDON at 06:08:04:599 on June 12, 2019
from https://pubs.acs.org/doi/10.1021/acsomega.8b00766.

© 2018 American Chemical Society

DOI: 10.1021/acsomega.8b00766
ACS Omega 2018, 3, 8655−8662

exfoliation processes are nanosheets with lateral size in the submicron range[27] and variable thicknesses ranging from single to few layers. The large lateral size of the flakes produced, control over thickness, and upscalability are characteristics of liquid exfoliation and make it advantageous over the other possible synthesis techniques such as hydrothermal thermal synthesis, microwave-assisted synthesis, or mechanical exfoliation.[28−30] A less investigated liquid-phase exfoliation route, which can produce high exfoliation yields of mono- and few-layered nanosheets preserving the lateral size close to 1 μm and larger,[2,3] is a two-step process with a first intercalation phase, followed by exfoliation. The lateral size of the nanosheets is a critical characteristic as it affects the electrical conductivity of thin films of restacked nanosheets. In this process, exfoliation is achieved via lithiation of layered compounds (either via $LiBH_4$ or via organolithium compounds),[31−35] followed by hydroxylation in water, where the bulk layered compound splits in its elementary building blocks. However, this exfoliation route if applied to TiS_2 would present significant challenges for ink production as the presence of water would oxidize TiS_2 via hydrolysis, leading to the formation of TiO_2.[13,36,37]

In this work, we develop a method to produce oxidation-resistant inks of few-layered TiS_2 nanosheets with lateral size greater than 1 μm and concentration up to 1 mg/mL. We established a nanosheet thickness−Raman active mode relationship for the first time, allowing the direct determination of the TiS_2 layer number through Raman spectroscopy. These advances pave the way for the development of electrodes that can utilize the attractive properties of TiS_2.

RESULTS AND DISCUSSION

TiS_2 nanosheets were produced from bulk TiS_2 powder via lithium borohydride intercalation, followed by exfoliation and separation in deionized water,[33,34] resulting in a colloidal suspension of highly exfoliated nanosheets (Figure 1a). Controllable thin-film morphologies, from isolated individual flakes (Figure S1a) to homogeneous thin films (thickness > 6 nm) (Figure 1b), were attained through the exploitation of liquid−liquid interfacial tension between hexane and water.[38,39]

Exciton peaks are not observed for monolayer TiS_2 because of its semimetallic band structure, which means that UV−vis spectroscopy cannot be used to quantitatively track the lateral size and layer number of the nanosheets as it is the case for semiconducting group VI TMDs.[24,40] Thus, more arduous atomic force and optical microscopies along with dynamic light scattering (DLS) were used to characterize the exfoliation quality. The thinnest flakes (Figures 1c and S1b,c) showed a consistent 2 nm height profile in atomic force microscopy (AFM), ascribed to a monolayer of TiS_2 when tip/sample interactions are accounted for.[41] Optical microscopy (OM) combined with contrast analysis (Figures 1d,e and S1a) demonstrated a distribution between one and six triatomic layers, centered at 3 layer thickness (Figure 1d,e). The related lateral sizes range from 1 to 10 μm, centered ∼3 μm at ∼2−3 layer thickness, with thicker flakes typically having larger lateral size (Figure 1e).

DLS, corrected for particle shape effects, corroborated the size distribution obtained by OM,[42] while showing a large distribution of submicron nanosheets that cannot be seen optically (Figure S2). From a combination of AFM, OM, and DLS, we can conclude that at least 13% of the stabilized nanosheets are monolayers, with a lateral size on the micrometer scale. A micrometer lateral size is crucial in order to fully characterize and utilize the properties of 2D layered materials.[43]

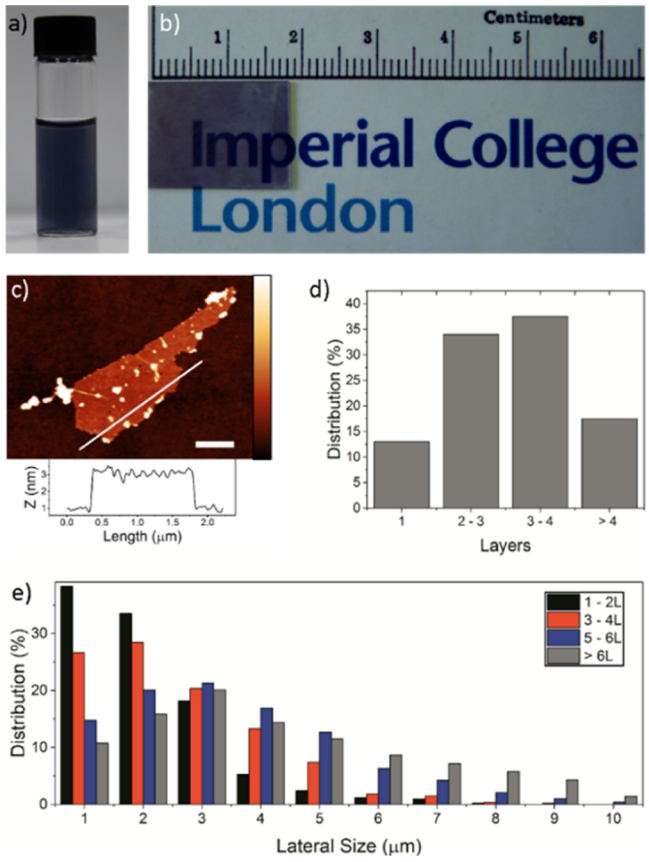


Figure 1. Photograph of (a) colloidal suspension of exfoliated TiS_2 nanosheets in water; (b) TiS_2 thin film deposited via dip-coating on a glass; (c) individualized 2 nm thick TiS_2 nanosheet (scale bar = 500 nm) (inset: cross-sectional height profile); (d) histogram of the TiS_2 layer number as determined by OM contrast analysis and the thickness is calibrated using WiTEC AFM for a given optical contrast—Figure S1; and (e) TiS_2 nanosheet lateral size separated by a number of layers as determined by OM (distribution is the percentage of flakes of a given layer number that falls within the lateral size regime).

Transmission electron microscopy (TEM) imaging (Figure 2) shows a crumpled, well-exfoliated, monolayer nanosheet with a lateral size of ∼4 μm and high crystal quality. In the bright-field TEM, TiS_2 nanosheets provide very faint phase contrast and become visible only at a sufficiently large defocus, indicating their ultrathin nature and supporting the OM and DLS analyses. The lattice spacing of 2.99 Å (Figure 2c) matches the predicted spacing for the (100) planes of 1T-TiS_2. The selected area electron diffraction (SAED) (Figure 2b) along the [001] zone axis clearly shows the lack of a diffuse amorphous ring and sharp intensities, confirming the high crystal quality, absence of oxidation, and the monolayer nature of the flake.[44] The combination of AFM, TEM, OM, and DLS has demonstrated the success of lithium borohydride exfoliation for TiS_2, producing monolayer flakes with a micrometer lateral size. However, it is highly desirable to expedite the exfoliation characterization process.

Raman spectroscopy is a powerful tool for rapidly characterizing the TMD exfoliation because of phonon stiffening in selected vibrational modes that are correlated with layer

DOI: 10.1021/acsomega.8b00766
ACS Omega 2018, 3, 8655−8662

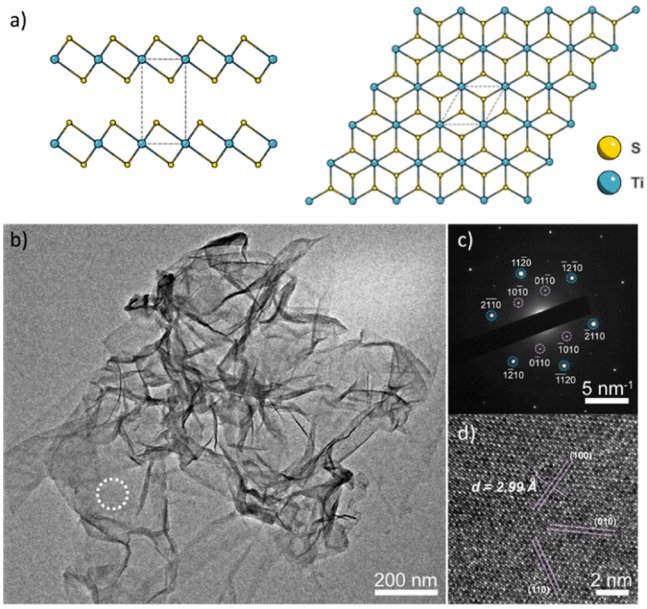


Figure 2. (a) Unit cell and crystal structure of 1T-TiS_2 (space group: $P\bar{3}m1$) and TEM analysis of a TiS_2 nanosheet exfoliated in water; (b) TEM image (highlighted area = SAED region); (c) electron diffraction pattern; and (d) atomic lattice in a high-resolution TEM image.

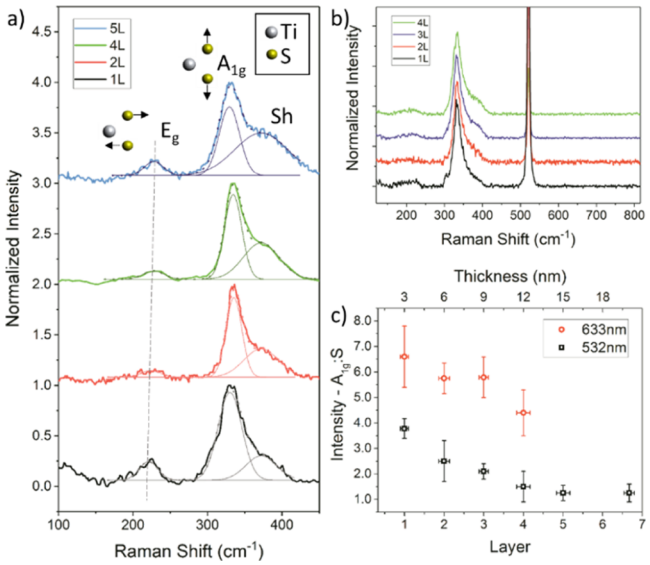


Figure 3. Raman spectroscopy of TiS_2 nanosheets deposited on SiO_2 (285 nm)/Si substrates via dip-coating (flake thickness determined via WiTEC-AFM): (a) spectra with intensity normalized to the A_{1g} peak and attained for different layer numbers using a 532 nm excitation laser (including a representation of A_{1g} and E_g vibrational modes), dashed line highlighting the minor change in E_g position with layer numbers; (b) spectra with intensity normalized to the A_{1g} peak and attained for different layer numbers using a 633 nm excitation laser; and (c) peak intensity ratio between the A_{1g} vibrational mode and the shoulder peak plotted as a function of layer numbers.

numbers.[45] 1T-TiS_2 is predicted to have two Raman active modes consisting of an in-plane vibrational mode (E_g) at 233 cm^{-1} and an out-of-plane mode (A_{1g}) at 328 cm^{-1} and two IR active modes (E_u) at 180 cm^{-1} and (A_{2u}) at 372 cm^{-1}.[46] Raman spectroscopy of both isolated flakes and thin films using a 532 nm laser revealed three primary peaks, 226 cm^{-1} (assigned to E_g), 330 cm^{-1} (assigned to A_{1g}), and a "shoulder peak" at ∼372 cm^{-1} (termed Sh herein) (Figure 3a).

Although this peak position coincides with the frequency of the A_{2u} mode, it cannot come from this vibrational mode. This shoulder peak has previously been reported for bulk and nanosheets of TiS_2,[47,48] and its origin has been attributed to defects in TiS_2, leading to an excess of interlayer metal atoms, which in turn causes a stiffening of the phonon modes[49,50] (Figure S3). If this holds, the shoulder peak should appear more pronounced for multilayers versus monolayers.

In order to probe if this stiffening can be used for the determination of layer numbers, confocal AFM/Raman studies were performed, with secondary AFM performed using a higher precision instrument as confirmation of our calibration (Figure S1).[41] This technique has allowed for the investigation of exfoliated TiS_2 nanosheets ranging from ∼1 to 6 layers (Figures S4 and S5).

The E_g peak displays a blue shift from 221 to 228 cm^{-1} from 1L (layer) to 4L (above which changes become indistinguishable) (Table S1, Figures S4 and S5) with the vibrational frequency approaching the E_g position of bulk TiS_2 at 233 cm^{-1}.[46] The stiffening of the E_g peak with the layer number is opposite to that observed for other TMDs.[51] The group VI TMDs most well characterized by Raman spectroscopy are thermodynamically stable in the 2H crystal structure, and octahedral 1T polymorphs are often only metastable and decay through energy minimization to 1T′ or Td.[52,53] Further, the Raman signal of 1T phase TMDs is predicted, and observed, to be significantly less intense than that of 2H phase TMDs of equivalent thickness samples.[54] The most commonly studied thermodynamically stable 1T TMD is TaS2, in which similar shifts in the E_g mode can be observed.[55,56] The reason for this blue shift is not clear, and we hypothesize that the presence of an excess of Ti intercalated between the nanosheets layers increases the interlayer interactions, thus stiffening the in-plane E_g mode.[57] This explanation is similar to that reported to cause the shoulder peak.[47,48] In contrast, the position of the A_{1g} vibrational mode does not present a significant trend with layer numbers ($\Delta\omega$ = 3 cm^{-1}, 5L−1L) (Table S1, Figures S4 and S5). The position of the shoulder peak is constant between 5L and 1L. The combination of these trends results in a $\Delta\omega$ (A_{1g} − E_g) of 104−108 cm^{-1} for 5L and 1L TiS_2 nanosheets, respectively. Although this trend is potentially useful, data fitting and interpretation over multiple flakes are difficult because of the broad full width at half-maximum (fwhm) and relatively low intensity of the E_g Raman mode. Therefore, understanding the more intense A_{1g} and shoulder modes are potentially more useful for the determination of layers.

Probing these more intense modes, we found that the intensity of the shoulder (Sh) peak at ∼372 cm^{-1} systematically increases with respect to the intensity of the A_{1g} mode with increasing thickness (Figure 3a,c). The peak intensity ratio A_{1g}/S ranges from 4 (1L) to 1.5 (5−7L) using 532 nm as the excitation wavelength and from 6.5 (1L) to 5 (4L) using 633 nm (Figure 3c). The relative change and overall intensity of the shoulder peak are significantly enhanced using a 532 nm laser as the excitation source compared to a 633 nm laser (Figure 3b); this appears to be due to the greater activation of the shoulder mode for all thicknesses using the 532 nm laser. The A_{1g}/S ratio of ∼1.25 found for nanosheets thicker than 5L does not decrease further because of its undistinguished nature from the bulk material. The relative increase in the intensity of 372 cm^{-1} peak with increasing thickness supports the

DOI: 10.1021/acsomega.8b00766
ACS Omega 2018, 3, 8655−8662

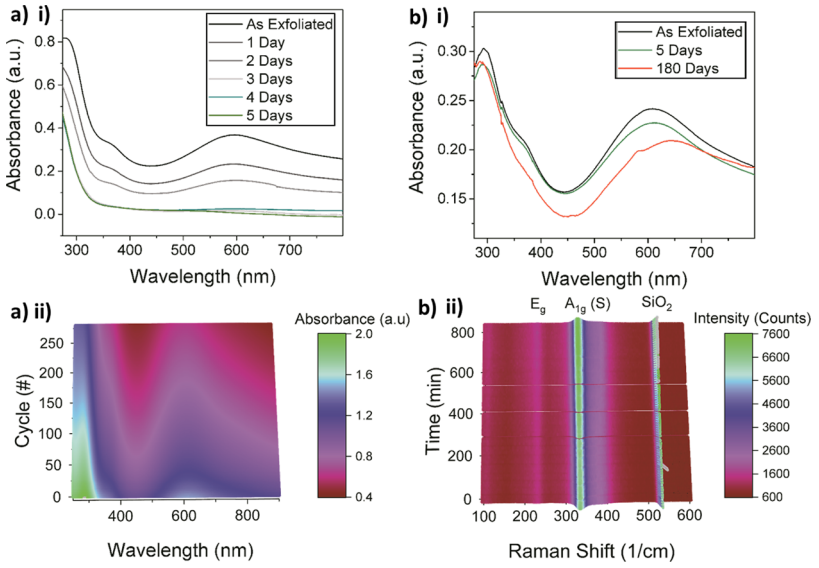


Figure 4. UV−vis absorption spectra of (a) exfoliated TiS_2 nanosheets in deoxygenated water over 5 days and (b) 20 nm thick films of TiS_2 nanosheets (from water exfoliation) recorded after deposition ("as deposited"), 5 days, and 180 days; (i) UV−vis spectra recorded over 24 h (1 cycle per 5 min) for a water suspension of TiS_2 immediately post exfoliation; and (ii) Raman spectra of a TiS_2 flake as a thin film over 800 min showing enhanced stability of TiS_2 on substrates.

hypothesis that the 372 cm^{-1} peak arises from an interlayer vibrational mode which could be due to excess interlayer metal atoms, causing a stiffening of the phonon. The fwhm increase with the layer number can be expected as each layer experiences a different relative load on the vibrational mode with increasing thickness, causing peak broadening. Raman mapping and AFM mapping of the same individual nanosheets using the 532 nm laser line show the consistency of the result across the entire individual nanosheet areas (Figure S5).

In order to make the TiS_2 nanosheet suspensions viable for applications, it is crucial to render this material chemically stable. Indeed, despite the high quality of the produced exfoliated nanosheets, these are rapidly destabilized by oxidation. Stability studies of the as-produced exfoliations were performed using both ζ-potential (ZP) measurements and UV−vis spectroscopy. The ZP of freshly exfoliated TiS_2 nanosheets in water showed a greater surface charge (−40 mV) compared to the nanosheets of MoS_2 (−35 mV) and WS_2 (−35 mV) in colloidal suspensions formed via the same exfoliation method. This can be attributed to the difference in electronegativity between S (2.58) and Ti (1.54) in TiS_2, which is higher compared to WS_2 and MoS_2 [W (2.36) and Mo (2.16)], leading to a stronger partial negative charge on the S atoms. Despite this initial stability, the TiS_2 suspension color was observed to convert to gray and then white over the course of 1 week. This color change was attributed to the local spontaneous conversion of TiS_2 to TiO_2 via the formation of intermediate TiSO species releasing H_2S gas as a byproduct of the reaction.[13,36,37]

UV−vis spectroscopy shows that the freshly exfoliated TiS_2 nanosheets in water exhibit two main absorption peaks at 294 and 600 nm and a smaller peak at 369 nm. Over a period of 5 days, the TiS_2 nanosheets undergo an initial agglomeration and precipitation stage, characterized by a decreased absorbance at 600 nm, followed by a blue shift of the 294 nm peak toward 266 nm (Figure 4a). This peak shift has been attributed to the oxidation of TiS_2 to TiO_2 as the peak at 266 nm arises from nanoparticles or nanosheets of TiO_2.[13,58,59] Furthermore, the decrease in the intensity of the 369 nm peak, which arises from a transition at the Γ point[60] of TiS_2, provides further confirmation of the conversion of TiS_2 to TiO_2 occurring in the solution. The 600 nm peak arises from an interband transition from near the Fermi level.[60−62] The position of these peaks has been attributed to the size of the TiS_2 nanosheets, with laterally smaller and thinner nanosheets, resulting in a blue-shifted peak.[61]

In order to probe the time scale of these effects, UV−vis spectroscopy was performed every 5 min on an exfoliation immediately post production for 24 h (280 cycles) (Figure 4a). This showed that even within a single day, significant aggregation and oxidation occurred within the solution, with the 600 nm peak decreasing dramatically in intensity representing instability in the solution. The 600 nm peak was also found to blue-shift slightly (611 nm at t = 0; 600 nm at t = 24 h), which is indicative of thinner nanosheets being stabilized in the solution. Further, there is a clear blue shift in the 294 nm peak within the first 12 h of measurement, indicating the early formation of oxide in the solution. This oxidation of TiS_2 in water is well-known, and we have observed the same effect in deoxygenated and oxygen-containing water. We can hypothesize that water molecules themselves cause this oxidation rather than dissolved O_2. Thus, utilizing the materials in applications is necessary to either process them to remove the solvent or change the dispersive solvent.

Solvent removal generally occurs upon fabricating thin films of exfoliated nanosheets.[39] Thin films of TiS_2 with a thickness of up to ∼20 nm were produced by dip-coating (Figure 1b) and had no observable red or blue shifting of any peaks after 5 days in air (Figure 4b), suggesting a good stability. This was confirmed by Raman spectroscopy on a single flake over 800 min, where no peak corresponding to TiO_2[63] was observed and the A_{1g}/Sh intensity ratio did not change. After being stored for 6 months in air, the ∼20 nm thick film demonstrated a splitting of the 600 nm peak into two peaks centered at 584 and 644 nm, respectively (Figure 4b). The splitting of the interband transition peak exhibiting a strong blue-shifted signal

DOI: 10.1021/acsomega.8b00766
ACS Omega 2018, 3, 8655−8662

at 584 nm provides evidence for the stability of mono and few over multilayered nanosheets. Although the presence of the highly red-shifted band at 644 nm suggests the retention of the thickest nanosheets, this dichotomy arises because of self-limiting oxidation for TMDs. In this case, the thick oxide layer acts as a passivation layer by preserving the structure of the underlying material.[64] Six nanometer thick films were also studied as a comparison; however, the signal intensity of these films was too low to analyze. In order to understand this peak splitting, a thin film of isolated flakes was immersed in water for 12 h. TiO_2 anatase Raman modes are observed to appear selectively at the edges of few-layered and multilayered flakes[63] (Figure S6) after this immersion, indicating that the counter-intuitively thicker flakes are more reactive. This observation supports the UV−vis blue shift of the 600 nm peak for TiS_2 exfoliations over 24 h.

To confirm this effect for the samples stored in air, X-ray diffraction (XRD) was used to study the thin films of 6 and 20 nm thickness. For both films, the position of the (001) peak at day 1 (Figure S7) shows a small increase in the interlayer distance compared to the bulk powders from 5.67 to 5.69 Å. The increase in the fwhm of the (001) peak from 0.3° to 0.1° of the bulk demonstrates a decrease in crystallite size, providing evidence of our well-exfoliated material. The (001) XRD peak of 6 nm thick films was unchanged over several weeks. Although the (001) peak of 20 nm thick films decreased exponentially over time (Figure S5), the shifting to larger interplanar distances also decreased. This different behavior between thicker and thinner films can be explained considering the exfoliation process. Recent studies on the pressure experienced by the molecules trapped in the interlayer van der Waals forces revealed that pressures up to 1.2 ± 0.3 GPa are generated, which can induce reactions or crystallization of molecules.[65] This suggest that the high pressure experienced by the H_2O, HO^-, and O_2 molecules in multilayered systems can provide the activation energy required for the observed oxidation to occur. This would also explain the stability of the monolayer nanosheets in comparison to multilayered nanosheets. Further films of 6 nm thickness were measured to have a sheet resistance of ∼2 kΩ/square immediately upon fabrication and after 180 days, demonstrating that thin-film processing can stabilize restacked TiS_2 films of 6 nm or less in thickness.

In order to retain the advantages of using the lithium exfoliation method in preserving a large lateral size of the flakes, we implemented a solvent exchange procedure whereby the water is replaced with NMP,[66] via a gravimetric centrifugation process. UV−vis absorption spectra of TiS_2 nanosheets suspended in NMP exhibit peaks at 295 and 349 nm as observed in water, which are stable over time (Figure 5). The interband transition peak (600 nm) is slightly blue-shifted compared to the water exfoliation (590 nm NMP, 596 nm water) (Table S2) as previously discussed; this blue shift indicates thinner nanosheets being stabilized in the solution, thus indicating that by solvent exchange with NMP, we are able to stabilize mono- and few-layered nanosheets (<3L) while it is less effective in stabilizing thicker nanosheets (>3L).[60,61,67]

The multilayered nanosheets are therefore more likely to be removed during a centrifugation cycle where we apply a lower speed to isolate well-exfoliated nanosheets in the supernatant and remove the precipitate. Over the course of 14 days, negligible changes in the UV−vis peak positions are observed,

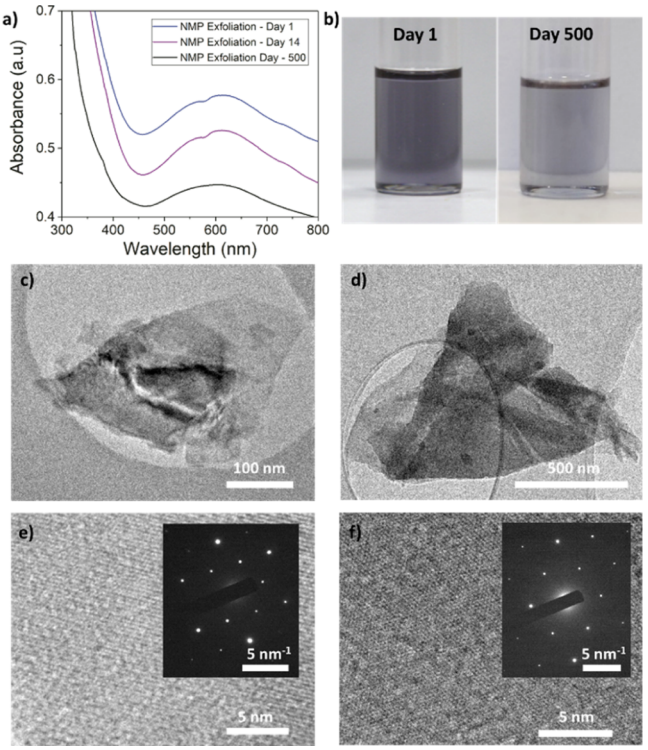


Figure 5. Lithium-based exfoliation of bulk TiS_2 in nanosheets stabilized via solvent exchange: (a) UV−vis absorption spectrum of TiS_2 nanosheets in 1-methyl-2-pyrollidone (NMP) as-prepared, after 14 days, and after 500 days; (b) photograph of aliquots of TiS_2 nanosheets stabilized in NMP as-produced and after 500 days; TEM image of TiS_2 stabilized via solvent exchange (c) as-produced and (d) after 500 days; and high-magnification imaging of (e) as-produced and (f) after 500 days (insets: SAED pattern).

with some decrease in intensity being attributed to aggregation and precipitation. After 500 days, the NMP−TiS_2 suspension showed equivalent peak positions for the 600 nm peak with a further decrease in intensity because of aggregation. The lack of oxide peaks supports the formation of stable TiS_2 inks in solution over 1 year. These stability results support the observations of Bissett et al. utilizing NMP for TiS_2 stabilization.[66] TEM and SAED (Figure 5c,d) of TiS_2 suspensions in NMP show the crystalline nature of the nanosheets and support the UV−vis spectroscopy observations of no change in the crystal structure over 500 days.

In conclusion, we have exfoliated oxidation-resistant nanosheets of TiS_2 down to monolayer thicknesses with lateral sizes up to 4 μm. This technique has allowed us to probe the effect of layer numbers on the Raman signal of TiS_2, providing a characterization tool for exfoliated material and thin films. Finally, we have demonstrated that via solvent exchange, it is possible to prevent the oxidation of TiS_2 flakes and to obtain highly concentrated (>1 mg/mL) inks stable for over 12 months. This study provides new insights into the exfoliation chemistry of TiS_2 and can accelerate the applications of nanosheets of TiS_2 from large area electronics to energy storage and energy conversion devices.

METHODS

Lithium Exfoliation. The TiS_2 nanosheets were obtained by the intercalation of lithium ions from $LiBH_4$ into TiS_2 powder (99.99%, Sigma-Aldrich, 200 mesh) (eq 1) with a

DOI: 10.1021/acsomega.8b00766
ACS Omega 2018, 3, 8655−8662

molar ratio of 2.5:1, followed by exfoliation via lithium hydration in water (eq 2)

$$LiBH_4 + TiS_{2(bulk)} \xrightarrow{\Delta} LiTiS_2 + \frac{1}{2}B_2H_6 + \frac{1}{2}H_2 \quad (1)$$

$$LiTiS_2 + H_2O \rightarrow TiS_{2(exf.)} + LiOH + \frac{1}{2}H_2 \quad (2)$$

Few- and monolayered TiS_2 were isolated from the multilayered and unexfoliated bulk material via centrifuging at speeds from 600 to 27 000 rpm (43−80 000g) in a Thermo Scientific Sorvall Lynx 6000 centrifuge.

Deoxygenated water was prepared by bubbling argon through water for 60 min prior to use. In addition, the water of the as-made suspension was deoxygenated by argon bubbling for 60 min.

Solvent Exchange. The TiS_2 nanosheets were stabilized in either 1-methyl-2-pyrrolidone (or 1-butyl-3-methylimidazolium hexafluorophosphate) via solvent exchange subsequent to lithium exfoliation. Immediately after exfoliation with deionized water, the exfoliated TiS_2 was centrifuged at 27 000 rpm for 30 min. The LiOH-containing supernatant was removed and replaced with either NMP or BMIM-PF_6, and the solution was agitated; this procedure was repeated five times to ensure the complete removal of water from the system. After the completion of solvent exchange, the standard centrifuge protocols were continued.

Dip-Coating. Exfoliated TiS_2 nanosheets were assembled to form thin films via dip-coating, exploiting the interfacial tension between hexane and water. Substrates were dipped into a vial containing 10 mL of deionized water and 1 mL hexane (Sigma-Aldrich), at pH 2 [controlled by introducing HCl 37% (Sigma-Aldrich)], and 3 mL of exfoliated TiS_2 in water suspension with 0.1 mg/mL of concentration. Continuous films with a thickness from ∼6 nm were obtained via tuning the drawing rate and dwell times.

Characterization. UV−vis spectroscopy was performed using a LAMBDA 25 UV−vis spectrometer and 1 cm path-length cuvettes. Scans were performed between 1100 and 250 nm at 2 nm/s with a spectral resolution of 0.5 nm. UV−vis characterization to assess the stability of exfoliated TiS_2 suspensions was performed overnight by running one scan every 5 min for 24 h. Low-volume cuvettes were utilized for stability studies of exfoliated TiS_2 nanosheets in BMIM-PF_6 samples.

Raman spectroscopy was performed using a WiTEC Raman-AFM system running Control Four software. Samples were analyzed on Si/SiO_2 substrates using an 1800 line/mm grating with both 532 and 632 nm lasers. Mapping was performed using a 300 nm step size with 0.5 s irradiation time per spectral point.

AFM mapping was performed using WiTEC AFM equipped with a reflex-coated arrow cantilever with a NC, 42 N/m spring constant, 285 kHz frequency tip. AFM mapping was also performed using Asylum MFP 3D AFM in ac air topography mode using a SiN PPP-NCHR 20 Nanosensor cantilever. OM was performed via a Zeiss AX10 optical microscope using a 100× objective. The resulting images were analyzed using ImageJ software for lateral size sorting and thickness determination. ZP measurements were obtained using Malvern Zetasizer Nano-Z using folded capillary cells. Measurements were performed on the TiS_2 supernatant solution subsequently to obtain gravimetric centrifugation. Scanning electron microscopy analysis of TiS_2 films was performed on a LEO Gemini field emission microscope.

The TEM images and SAED patterns were acquired using a JEOL JEM-2100F microscope operated at an accelerating voltage of 200 kV.

The XRD patterns of TiS_2 films were studied via a PANalytical X'Pert Pro diffractometer. Scans were performed from 5 to 80° 2θ with a step size of 0.033°. X'Pert Highscore plus software was used to match the database.

■ ASSOCIATED CONTENT

Supporting Information

The Supporting Information is available free of charge on the ACS Publications website at DOI: 10.1021/acsomega.8b00766.

AFM calibration results; DLS size calibration; proposed vibrational schematic for interstitial Ti atoms; Raman laser peak shift (532 nm) with layer numbers; confocal optical, Raman, and AFM signal for individual TiS_2 nanosheets; Raman peak fitting parameters; Raman of edge oxidation of TiS_2; XRD of thin-film stability; solvent exchange exfoliation and stabilization; and UV−vis peak positions (PDF)

■ AUTHOR INFORMATION

Corresponding Author

*E-mail: c.mattevi@imperial.ac.uk (C.M.).

ORCID

Peter C. Sherrell: 0000-0003-4644-6238
Federico M. Pesci: 0000-0003-2558-2222
Cecilia Mattevi: 0000-0003-0005-0633

Author Contributions

C.M. conceptualized the project and designed the experiments. P.C.S. wrote the manuscript, analyzed the data, and performed Raman spectroscopy and XRD experiments. K.S. performed AFM using the WiTEC Raman/AFM system. C.G. optimized the exfoliation procedure and performed initial exfoliations of TiS_2 in water. J.R. performed UV−vis experiments and performed data analysis on confocal Raman/AFM experiments. M.S.S. performed TEM imaging and analysis and UV−vis data analysis. F.M.P. performed lithium intercalation and exfoliation for solvent exchange and thin-film deposition. P.P. performed and analyzed time-resolved Raman experiments. V.L.B. performed high-resolution AFM for images and calibration. All authors have read and approved the manuscript.

Notes

The authors declare no competing financial interest.

■ ACKNOWLEDGMENTS

The authors acknowledge the use of characterization facilities within the Harvey Flower Electron Microscopy Suite, XRD suite, and AFM suite, Department of Materials, Imperial College London. M.S.S. would like to acknowledge the President's PhD Scholarship programme at Imperial College London for financial support. C.M. would like to acknowledge the EPSRC awards, EP/K01658X/1, EP/K016792/1, and EP/M022250/1, the EPSRC-Royal Society Fellowship Engagement Grant EP/L003481/1, and the award of a Royal Society University Research Fellowship by the UK Royal Society.

DOI: 10.1021/acsomega.8b00766
ACS Omega 2018, 3, 8655−8662

REFERENCES

(1) Novoselov, K. S.; Jiang, D.; Schedin, F.; Booth, T. J.; Khotkevich, V. V.; Morozov, S. V.; Geim, A. K. Two-dimensional atomic crystals. *Proc. Natl. Acad. Sci. U.S.A.* **2005**, *102*, 10451−10453.

(2) Wang, Q. H.; Kalantar-Zadeh, K.; Kis, A.; Coleman, J. N.; Strano, M. S. Electronics and optoelectronics of two-dimensional transition metal dichalcogenides. *Nat. Nanotechnol.* **2012**, *7*, 699−712.

(3) Chhowalla, M.; Jena, D.; Zhang, H. Two-dimensional semiconductors for transistors. *Nat. Rev. Mater.* **2016**, *1*, 16052.

(4) Whittingham, M. S. Electrical Energy Storage and Intercalation Chemistry. *Science* **1976**, *192*, 1126−1127.

(5) Ĉaja, J.; Kaner, R. B.; MacDiarmid, A. G. A Rechargeable Battery Employing a Reduced Polyacetylene Anode and a Titanium Disulfide Cathode. *J. Electrochem. Soc.* **1984**, *131*, 2744.

(6) Holleck, G. L.; Driscoll, J. R. Transition metal sulfides as cathodes for secondary lithium batteries-II. titanium sulfides. *Electrochim. Acta* **1977**, *22*, 647−655.

(7) Seh, Z. W.; Sun, Y.; Zhang, Q.; Cui, Y. Designing high-energy lithium-sulfur batteries. *Chem. Soc. Rev.* **2016**, *45*, 5605−5634.

(8) Xu, C.; Brown, P. A.; Shuford, K. L. Strain-induced semimetal-to-semiconductor transition and indirect-to-direct band gap transition in monolayer 1T-TiS_2. *RSC Adv.* **2015**, *5*, 83876−83879.

(9) Fang, C. M.; de Groot, R. A.; Haas, C. Bulk and surface electronic structure of 1T−TiS_2 and 1T−$TiSe_2$. *Phys. Rev. B: Condens. Matter Mater. Phys.* **1997**, *56*, 4455−4463.

(10) Riekel, C.; Schöllhorn, R. Structure refinement of non-stoichiometric TiS_2. *Mater. Res. Bull.* **1975**, *10*, 629−633.

(11) Wilson, J. A. Concerning the semimetallic characters of TiS_2 and $TiSe_2$. *Solid State Commun.* **1977**, *22*, 551−553.

(12) Benard, J.; Jeannin, Y. Investigations of Nonstoichiometric Sulfides. *Nonstoichiometric Compounds*; American Chemical Society, 1963; Vol. *39*, pp 191−203.

(13) Park, K. H.; Choi, J.; Kim, H. J.; Oh, D.-H.; Ahn, J. R.; Son, S. U. Unstable Single-Layered Colloidal TiS_2 Nanodisks. *Small* **2008**, *4*, 945−950.

(14) Mahuli, N.; Sarkar, S. K. Atomic layer deposition of titanium sulfide and its application in extremely thin absorber solar cells. *J. Vac. Sci. Technol., A* **2015**, *33*, 01A150.

(15) Ivanovskaya, V. V.; Seifert, G.; Ivanovskii, A. L. Electronic structure of titanium disulfide nanostructures: Monolayers, nanostripes, and nanotubes. *Semiconductors* **2005**, *39*, 1058−1065.

(16) Chen, J.; Li, S.-L.; Tao, Z.-L.; Shen, Y.-T.; Cui, C.-X. Titanium Disulfide Nanotubes as Hydrogen-Storage Materials. *J. Am. Chem. Soc.* **2003**, *125*, 5284−5285.

(17) Yang, Y.; Zheng, G.; Cui, Y. Nanostructured sulfur cathodes. *Chem. Soc. Rev.* **2013**, *42*, 3018−3032.

(18) Muller, G. A.; Cook, J. B.; Kim, H.-S.; Tolbert, S. H.; Dunn, B. High Performance Pseudocapacitor Based on 2D Layered Metal Chalcogenide Nanocrystals. *Nano Lett.* **2015**, *15*, 1911−1917.

(19) Whittingham, M. Insertion electrodes as SMART materials: the first 25 years and future promises. *Solid State Ionics* **2000**, *134*, 169−178.

(20) Trevey, J. E.; Stoldt, C. R.; Lee, S.-H. High Power Nanocomposite TiS_2 Cathodes for All-Solid-State Lithium Batteries. *J. Electrochem. Soc.* **2011**, *158*, A1282.

(21) Zhang, X.; Qiao, X.-F.; Shi, W.; Wu, J.-B.; Jiang, D.-S.; Tan, P.-H. Phonon and Raman scattering of two-dimensional transition metal dichalcogenides from monolayer, multilayer to bulk material. *Chem. Soc. Rev.* **2015**, *44*, 2757−2785.

(22) Late, D. J.; Huang, Y.-K.; Liu, B.; Acharya, J.; Shirodkar, S. N.; Luo, J.; Yan, A.; Charles, D.; Waghmare, U. V.; Dravid, V. P.; Rao, C. N. R. Sensing Behavior of Atomically Thin-Layered MoS_2 Transistors. *ACS Nano* **2013**, *7*, 4879−4891.

(23) Late, D. J.; Liu, B.; Matte, H. S. S. R.; Rao, C. N. R.; Dravid, V. P. Rapid Characterization of Ultrathin Layers of Chalcogenides on SiO_2/Si Substrates. *Adv. Funct. Mater.* **2012**, *22*, 1894−1905.

(24) Backes, C.; Higgins, T. M.; Kelly, A.; Boland, C.; Harvey, A.; Hanlon, D.; Coleman, J. N. Guidelines for Exfoliation, Characterization and Processing of Layered Materials Produced by Liquid Exfoliation. *Chem. Mater.* **2016**, *29*, 243−255.

(25) O'Neill, A.; Khan, U.; Coleman, J. N. Preparation of High Concentration Dispersions of Exfoliated MoS_2 with Increased Flake Size. *Chem. Mater.* **2012**, *24*, 2414−2421.

(26) Yao, Y.; Tolentino, L.; Yang, Z.; Song, X.; Zhang, W.; Chen, Y.; Wong, C.-p. High-Concentration Aqueous Dispersions of MoS_2. *Adv. Funct. Mater.* **2013**, *23*, 3577−3583.

(27) Yu, X.; Prévot, M. S.; Sivula, K. Multiflake Thin Film Electronic Devices of Solution Processed 2D MoS_2 Enabled by Sonopolymer Assisted Exfoliation and Surface Modification. *Chem. Mater.* **2014**, *26*, 5892−5899.

(28) Manzeli, S.; Ovchinnikov, D.; Pasquier, D.; Yazyev, O. V.; Kis, A. 2D transition metal dichalcogenides. *Nat. Rev. Mater.* **2017**, *2*, 17033.

(29) Lv, R.; Robinson, J. A.; Schaak, R. E.; Sun, D.; Sun, Y.; Mallouk, T. E.; Terrones, M. Transition Metal Dichalcogenides and Beyond: Synthesis, Properties, and Applications of Single- and Few-Layer Nanosheets. *Acc. Chem. Res.* **2015**, *48*, 56−64.

(30) Sokolikova, M. S.; Sherrell, P. C.; Palczynski, P.; Bemmer, V. L.; Mattevi, C. Room-temperature growth of colloidal Bi2Te3 nanosheets. *Chem. Commun.* **2017**, *53*, 8026.

(31) Eda, G.; Yamaguchi, H.; Voiry, D.; Fujita, T.; Chen, M.; Chhowalla, M. Photoluminescence from Chemically Exfoliated MoS_2. *Nano Lett.* **2011**, *11*, 5111−5116.

(32) Joensen, P.; Frindt, R. F.; Morrison, S. R. Single-layer MoS_2. *Mater. Res. Bull.* **1986**, *21*, 457−461.

(33) Tsai, H.-L.; Heising, J.; Schindler, J. L.; Kannewurf, C. R.; Kanatzidis, M. G. Exfoliated−Restacked Phase of WS_2. *Chem. Mater.* **1997**, *9*, 879−882.

(34) Heising, J.; Kanatzidis, M. G. Exfoliated and Restacked MoS_2 and WS_2: Ionic or Neutral Species? Encapsulation and Ordering of Hard Electropositive Cations. *J. Am. Chem. Soc.* **1999**, *121*, 11720−11732.

(35) Yuwen, L.; Yu, H.; Yang, X.; Zhou, J.; Zhang, Q.; Zhang, Y.; Luo, Z.; Su, S.; Wang, L. Rapid preparation of single-layer transition metal dichalcogenide nanosheets via ultrasonication enhanced lithium intercalation. *Chem. Commun.* **2016**, *52*, 529−532.

(36) Cucinotta, C. S.; Dolui, K.; Pettersson, H.; Ramasse, Q. M.; Long, E.; O'Brian, S. E.; Nicolosi, V.; Sanvito, S. Electronic Properties and Chemical Reactivity of TiS_2 Nanoflakes. *J. Phys. Chem. C* **2015**, *119*, 15707−15715.

(37) Martinez, H.; Auriel, C.; Gonbeau, D.; Loudet, M.; Pfister-Guillouzo, G. Studies of 1T TiS_2 by STM, AFM and XPS: the mechanism of hydrolysis in air. *Appl. Surf. Sci.* **1996**, *93*, 231−235.

(38) Divigalpitiya, W. M. R.; Morrison, S. R.; Frindt, R. F. Thin oriented films of molybdenum disulphide. *Thin Solid Films* **1990**, *186*, 177−192.

(39) Pesci, F. M.; Sokolikova, M. S.; Grotta, C.; Sherrell, P. C.; Reale, F.; Sharda, K.; Ni, N.; Palczynski, P.; Mattevi, C. MoS_2/WS_2 Heterojunction for Photoelectrochemical Water Oxidation. *ACS Catal.* **2017**, *7*, 4990−4998.

(40) Backes, C.; Smith, R. J.; McEvoy, N.; Berner, N. C.; McCloskey, D.; Nerl, H. C.; O'Neill, A.; King, P. J.; Higgins, T.; Hanlon, D. Edge and confinement effects allow in situ measurement of size and thickness of liquid-exfoliated nanosheets. *Nat. Commun.* **2014**, *5*, 4576.

(41) Backes, C.; Smith, R. J.; McEvoy, N.; Berner, N. C.; McCloskey, D.; Nerl, H. C.; O'Neill, A.; King, P. J.; Higgins, T.; Hanlon, D.; Scheuschner, N.; Maultzsch, J.; Houben, L.; Duesberg, G. S.; Donegan, J. F.; Nicolosi, V.; Coleman, J. N. Edge and confinement effects allow in situ measurement of size and thickness of liquid-exfoliated nanosheets. *Nat. Commun.* **2014**, *5*, 4576.

(42) Lotya, M.; Rakovich, A.; Donegan, J. F.; Coleman, J. N. Measuring the lateral size of liquid-exfoliated nanosheets with dynamic light scattering. *Nanotechnology* **2013**, *24*, 265703.

(43) Yu, X.; Sivula, K. Toward Large-Area Solar Energy Conversion with Semiconducting 2D Transition Metal Dichalcogenides. *ACS Energy Lett.* **2016**, *1*, 315−322.

DOI: 10.1021/acsomega.8b00766
ACS Omega 2018, 3, 8655−8662

(44) Wu, R. J.; Odlyzko, M. L.; Mkhoyan, K. A. Determining the thickness of atomically thin MoS_2 and WS_2 in the TEM. *Ultramicroscopy* **2014**, *147*, 8−20.
(45) Zhang, X.; Tan, Q.-H.; Wu, J.-B.; Shi, W.; Tan, P.-H. Review on the Raman spectroscopy of different types of layered materials. *Nanoscale* **2016**, *8*, 6435−6450.
(46) Dolui, K.; Sanvito, S. Dimensionality-driven phonon softening and incipient charge density wave instability in TiS2. *Europhys. Lett.* **2016**, *115*, 47001.
(47) Lin, C.; Zhu, X.; Feng, J.; Wu, C.; Hu, S.; Peng, J.; Guo, Y.; Peng, L.; Zhao, J.; Huang, J.; Yang, J.; Xie, Y. Hydrogen-Incorporated TiS_2 Ultrathin Nanosheets with Ultrahigh Conductivity for Stamp-Transferrable Electrodes. *J. Am. Chem. Soc.* **2013**, *135*, 5144−5151.
(48) Let, A. L.; Mainwaring, D. E.; Rix, C.; Murugaraj, P. Thio sol-gel synthesis of titanium disulfide thin films and powders using titanium alkoxide precursors. *J. Non-Cryst. Solids* **2008**, *354*, 1801−1807.
(49) Klipstein, P. C.; Bagnall, A. G.; Liang, W. Y.; Marseglia, E. A.; Friend, R. H. Stoichiometry dependence of the transport properties of TiS_2. *J. Phys. C: Solid State Phys.* **1981**, *14*, 4067−4081.
(50) Smith, J. E.; Nathan, M. I.; Shafer, M. W.; Torrance, J. *Proceedings 11th Conference on Semiconductors*, 1972; pp 1306−1311.
(51) Lee, C.; Yan, H.; Brus, L. E.; Heinz, T. F.; Hone, J.; Ryu, S. Anomalous Lattice Vibrations of Single- and Few-Layer MoS_2. *ACS Nano* **2010**, *4*, 2695−2700.
(52) Ma, F.; Gao, G.; Jiao, Y.; Gu, Y.; Bilic, A.; Zhang, H.; Chen, Z.; Du, A. Predicting a new phase (T″) of two-dimensional transition metal di-chalcogenides and strain-controlled topological phase transition. *Nanoscale* **2016**, *8*, 4969−4975.
(53) Duerloo, K.-A. N.; Li, Y.; Reed, E. J. Structural phase transitions in two-dimensional Mo- and W-dichalcogenide monolayers. *Nat. Commun.* **2014**, *5*, 4214.
(54) Fan, X.; Xu, P.; Zhou, D.; Sun, Y.; Li, Y. C.; Nguyen, M. A. T.; Terrones, M.; Mallouk, T. E. Fast and Efficient Preparation of Exfoliated 2H MoS_2 Nanosheets by Sonication-Assisted Lithium Intercalation and Infrared Laser-Induced 1T to 2H Phase Reversion. *Nano Lett.* **2015**, *15*, 5956−5960.
(55) Fu, W.; Chen, Y.; Lin, J.; Wang, X.; Zeng, Q.; Zhou, J.; Zheng, L.; Wang, H.; He, Y.; He, H.; Fu, Q.; Suenaga, K.; Yu, T.; Liu, Z. Controlled Synthesis of Atomically Thin 1T-TaS_2 for Tunable Charge Density Wave Phase Transitions. *Chem. Mater.* **2016**, *28*, 7613−7618.
(56) Zhao, R.; Wang, Y.; Deng, D.; Luo, X.; Lu, W. J.; Sun, Y.-P.; Liu, Z.-K.; Chen, L.-Q.; Robinson, J. Tuning Phase Transitions in 1T-TaS_2 via the Substrate. *Nano Lett.* **2017**, *17*, 3471−3477.
(57) Ishii, M.; Saeki, M.; Kawada, I. Raman Study of Non-Stoichiometric Titanium Sulfides. *Phys. Status Solidi B* **1984**, *124*, K109−K112.
(58) Liu, Y.; Claus, R. O. Blue Light Emitting Nanosized TiO_2 Colloids. *J. Am. Chem. Soc.* **1997**, *119*, 5273−5274.
(59) Ghosh, H. N.; Adhikari, S. Trap State Emission from TiO_2 Nanoparticles in Microemulsion Solutions. *Langmuir* **2001**, *17*, 4129−4130.
(60) Beal, A. R.; Knights, J. C.; Liang, W. Y. Transmission spectra of some transition metal dichalcogenides. I. Group IVA: octahedral coordination. *J. Phys. C: Solid State Phys.* **1972**, *5*, 3531−3539.
(61) Rossi, D.; Han, J. H.; Yoo, D.; Dong, Y.; Park, Y.; Cheon, J.; Son, D. H. Photoinduced Separation of Strongly Interacting 2-D Layered TiS_2 Nanodiscs in Solution. *J. Phys. Chem. C* **2014**, *118*, 12568−12573.
(62) Yun, W. S.; Han, S. W.; Hong, S. C.; Kim, I. G.; Lee, J. D. Thickness and strain effects on electronic structures of transition metal dichalcogenides: 2H-MX_2 semiconductors (M = Mo, W; X = S, Se, Te). *Phys. Rev. B: Condens. Matter Mater. Phys.* **2012**, *85*, 033305.
(63) Zhang, W. F.; He, Y. L.; Zhang, M. S.; Yin, Z.; Chen, Q. Raman scattering study on anatase TiO_2 nanocrystals. *J. Phys. D: Appl. Phys.* **2000**, *33*, 912−916.
(64) Yamamoto, M.; Dutta, S.; Aikawa, S.; Nakaharai, S.; Wakabayashi, K.; Fuhrer, M. S.; Ueno, K.; Tsukagoshi, K. Self-Limiting Layer-by-Layer Oxidation of Atomically Thin WSe_2. *Nano Lett.* **2015**, *15*, 2067−2073.
(65) Vasu, K. S.; Prestat, E.; Abraham, J.; Dix, J.; Kashtiban, R. J.; Beheshtian, J.; Sloan, J.; Carbone, P.; Neek-Amal, M.; Haigh, S. J.; Geim, A. K.; Nair, R. R. Van der Waals pressure and its effect on trapped interlayer molecules. *Nat. Commun.* **2016**, *7*, 12168.
(66) Bissett, M. A.; Worrall, S. D.; Kinloch, I. A.; Dryfe, R. A. W. Comparison of Two-Dimensional Transition Metal Dichalcogenides for Electrochemical Supercapacitors. *Electrochim. Acta* **2016**, *201*, 30−37.
(67) Jeong, S.; Yoo, D.; Ahn, M.; Miró, P.; Heine, T.; Cheon, J. Tandem intercalation strategy for single-layer nanosheets as an effective alternative to conventional exfoliation processes. *Nat. Commun.* **2015**, *6*, 5763.

DOI: 10.1021/acsomega.8b00766
ACS Omega 2018, 3, 8655−8662